

ChimeraLM detects amplification artifacts for
accurate structural variant calling in long-read
single-cell sequencing

Yangyang Li^{1†}, Qingxiang Guo^{1†}, Rendong Yang^{1,2*}

¹Department of Urology, Northwestern University Feinberg School of Medicine, 303 E Superior St, Chicago, 60611, IL, USA.

²Robert H. Lurie Comprehensive Cancer Center, Northwestern University Feinberg School of Medicine, 675 N St Clair St, Chicago, 60611, IL, USA.

*Corresponding author(s). E-mail(s): rendong.yang@northwestern.edu;

Contributing authors: yangyang.li@northwestern.edu;

qingxiang.guo@northwestern.edu;

†These authors contributed equally to this work.

Abstract

Single-cell genomic analysis relies on Whole Genome Amplification (WGA) to generate sufficient DNA for sequencing, but this process introduces chimeric artifacts that manifest as false-positive Structural Variations (SVs) and compromise downstream interpretation. Here we present ChimeraLM, a genomic language model that identifies and removes WGA-induced chimeric reads from long-read sequencing data. ChimeraLM uses a model architecture based on Hyena operators to analyze DNA sequences at single-nucleotide resolution, learning generalizable sequence features that distinguish genuine biological sequences from amplification-induced artifacts. When applied to nanopore sequencing data from WGA-amplified cells, ChimeraLM reduces chimeric read content by approximately 90% while retaining 87-92% of true SVs. This filtering improves SV validation rates 10-16 fold and normalizes SV type distributions toward bulk sequencing profiles, eliminating the characteristic false-positive inversion (INV) bias in unprocessed WGA data. Attention weight analysis reveals that ChimeraLM can focus on chimeric junction regions, learning biologically interpretable sequence features. ChimeraLM addresses a fundamental bottleneck in single-cell genomics,

047 enabling more confident detection of chromosomal instability and **SV** in appli-
048 cations across cancer biology, developmental biology, and neuroscience. The
049 software is available at <https://github.com/ylab-hi/ChimeraLM>.

050 **Keywords:** Whole Genome Amplification, Single Cell, Genomic Language Model,
051 Structural Variation

052

053

054

055 Main

056

057 Single-cell genomics has revolutionized our understanding of cellular heterogeneity by
058 enabling characterization of individual cells rather than bulk populations [? ? ? ?].
059 This approach has proven instrumental in uncovering rare cell types [?], tracking
060 developmental trajectories [?], and elucidating tumor evolution through clonal archi-
061 tecture analysis. However, the limited DNA content in a single cell—typically only
062 6–7 picograms containing approximately two copies of the 3-billion-base-pair human
063 genome—poses significant technical challenges for comprehensive genomic analysis [? ? ?].
064 To overcome this limitation, **WGA** has become essential for single-cell genomic
065 studies [? ? ? ? ?]. Various **WGA** techniques have been developed, each with dis-
066 tinct amplification mechanisms and characteristic error profiles. **Multiple Displacement**
067 **Amplification (MDA)**, introduced by Dean et al. [?], utilizes the highly processive
068 phi29 DNA polymerase to achieve isothermal amplification with products exceeding 10
069 kb, though it suffers from pronounced amplification bias and chimera formation [? ?].
070 **Degenerate Oligonucleotide-Primed PCR (DOP-PCR)**, pioneered by Telenius et al. [?]
071 , employs thermocycling with degenerate primers to achieve more uniform coverage
072 but generates shorter amplicons. **Multiple Annealing and Looping-based Amplification**
073 **Cycles (MALBAC)** combines quasi-linear preamplification with exponential amplifica-
074 tion to reduce bias [?], while **Linear Amplification via Transposon Insertion (LIANTI)**
075 uses transposon insertion to create defined amplification origins, significantly improv-
076 ing uniformity and reducing artifacts [?]. More recently, **Primary Template-directed**
077 **Amplification (PTA)** [?] and **droplet-based MDA (dMDA)** [? ?] have emerged as
078 promising alternatives that modify reaction conditions to suppress chimera forma-
079 tion, though these methods require specialized equipment and protocols that have
080 limited their widespread adoption. These amplification methods can increase DNA
081 content by several orders of magnitude (typically 1,000- to 10,000-fold), generating
082 sufficient material for high-coverage sequencing necessary for reliable variant calling,
083 copy number analysis, and **SV** detection [? ? ? ? ? ?].

084

085 Accurate single-cell genomics is particularly critical for multiple applications where
086 false-positive **SVs** can lead to incorrect biological conclusions. In cancer research, dis-
087 tinguishing genuine clonal evolution patterns from amplification artifacts is essential
088 for understanding tumor heterogeneity and therapeutic resistance [?]. In develop-
089 mental biology, accurate detection of somatic mosaicism enables the reconstruc-
090 tion of lineage relationships and identification of pathogenic mutations in rare cell pop-
091 ulations. For CRISPR-based genome editing, single-cell analysis with reliable **SV**
092 detection is crucial for comprehensive assessment of off-target effects and ensuring

genomic stability [?]. However, false-positive SVs introduced during amplification can confound these analyses, leading to misinterpretation of genomic rearrangements and their biological significance [? ?].	093
	094
	095
Despite its critical role, WGA introduces systematic artifacts that significantly impact downstream analyses [? ? ? ? ?]. Among the most problematic are chimeric sequences—artificial DNA constructs formed through template switching during amplification. During MDA , the highly processive phi29 polymerase can dissociate from one genomic template and reinitiate synthesis on a spatially proximate but genetically distant template [? ?]. This phenomenon is exacerbated by the branching nature of MDA , where multiple DNA synthesis reactions occur simultaneously in a densely packed reaction environment, increasing the probability of illegitimate template switching [?]. Critically, even with WGA technological advances, chimeric artifacts remain highly prevalent in single-cell long-read sequencing data [? ?]. Lasken and Stockwell [?] demonstrated that chimera formation occurs through both strand displacement and branch migration mechanisms, with chimeric junctions often occurring at sites of microhomology. These chimeric artifacts manifest as apparent SVs —including deletions (DELs) , insertions (INSs) , INVs , and translocations (TRAs) —that do not exist in the original cell [? ?], posing substantial challenges for accurate SV detection in single-cell studies. Early work by Pinard et al. [?] documented significant amplification bias and the presence of chimeric products in MDA , demonstrating that certain genomic regions can be over- or under-represented by orders of magnitude.	096
	097
	098
	099
	100
	101
	102
	103
	104
	105
	106
	107
	108
	109
	110
	111
	112
	113
	114
The advent of long-read sequencing technologies, particularly Pacific Biosciences (PacBio) and Oxford Nanopore Technologies (ONT) platforms, has transformed SV detection by enabling direct observation of structural rearrangements that span kilobases to megabases. Numerous computational tools have been developed to detect SVs from long-read data, including Sniffles2 [? ?], DeBreak [?], SVIM [?], and cuteSV [?]. These methods typically employ read alignment analysis, split-read detection, and local assembly strategies to identify SV signatures [?]. However, distinguishing genuine biological SVs from WGA -induced chimeric artifacts remains challenging [? ? ? ?].	115
	116
	117
	118
	119
	120
	121
	122
	123
Current computational approaches for identifying WGA -induced artifacts rely primarily on coverage-based metrics and read-pair orientation patterns [? ?]. However, these heuristic methods often fail to distinguish genuine SVs from amplification artifacts, particularly when chimeric sequences exhibit complex rearrangement patterns, occur in repetitive genomic regions, or involve multiple genomic loci [? ?]. This lack of robust, automated artifact detection has limited the reliability of SV analysis in single-cell studies and hindered the full realization of single-cell genomics' potential for studying somatic mosaicism, tumor evolution, and rare cell populations.	124
	125
	126
	127
	128
	129
	130
	131
The emergence of deep learning, particularly language models based on transformer architectures, has demonstrated remarkable success in genomics applications [? ? ? ?]. Recent genomic language models have shown the ability to learn complex sequence patterns and contextual relationships in DNA sequences, enabling improved performance in tasks such as regulatory element prediction, variant effect prediction, and functional annotation [? ? ?]. These models treat DNA sequences analogously	132
	133
	134
	135
	136
	137
	138

139 to natural language, learning representations that capture both local motifs and long-
140 range dependencies [?]. By training on large-scale genomic datasets, such models can
141 internalize patterns of genuine biological sequences, including characteristic features
142 of repetitive elements, chromatin structure, and sequence composition biases.

143 Here, we developed ChimeraLM, a genomic language model specifically designed
144 to detect chimeric artifacts introduced by **WGA**. By leveraging deep learning to cap-
145 ture sequence patterns, structural features, and contextual information in genomic
146 reads [? ? ? ? ?], ChimeraLM effectively distinguishes genuine biological sequences
147 from **WGA**-induced chimeric artifacts. We demonstrate that ChimeraLM achieves
148 superior performance compared to existing methods and substantially improves the
149 reliability of **SV** detection in single-cell genomic studies, thereby enabling accurate SV
150 analysis at single-cell resolution.

151

152 Results

153

154 Overview of ChimeraLM workflow and model architecture

155

156 Single-cell genomics relies on whole-genome amplification (**WGA**) to obtain sufficient
157 DNA for sequencing (Fig. 1a). The standard workflow includes single-cell isolation,
158 DNA extraction, **WGA**, long-read sequencing (e.g., **ONT**), base calling, and alignment
159 to the reference genome. During amplification, template-switching events introduce
160 artificial chimeric reads, resulting in alignment files that contain a mixture of authentic
161 and artifactual sequences. In downstream analysis, these artifacts can mimic **SV** and
162 confound variant detection. To address this challenge, we developed ChimeraLM, a
163 **Genomic Language Model (GLM)** designed to integrate directly into this analysis
164 pipeline and distinguish biological reads from amplification-induced artifacts.

165 ChimeraLM functions as a pre-processing filter, operating after read alignment
166 but before **SV** detection. It evaluates each chimeric read—sequences with multiple
167 alignments to distant genomic locations—and classifies it as either biological (genuine)
168 or artificial (**WGA**-induced). This binary decision enables the retention of authentic
169 genomic sequences while removing amplification artifacts prior to variant calling. The
170 resulting high-confidence biological reads are then passed to conventional **SV** detection
171 algorithms for accurate identification of genomic rearrangements.

172 A high-confidence labeled dataset was required for supervised training of the model
173 (Fig. 1b). We constructed this dataset using sequencing data from the PC3 prostate
174 cancer cell line, which provides both **WGA**-amplified and non-amplified (bulk) genomic
175 data. The key assumption is that bulk sequencing contains only genuine genomic
176 sequences, whereas **WGA** data includes both genuine and artificial chimeras. Chimeric
177 reads from the PC3 **WGA** PromethION dataset were systematically compared against
178 three independent bulk datasets (**ONT** PromethION, **ONT** MinION, and PacBio; see
179 **Methods**). **WGA** reads whose chimeric structures were absent from all three bulk
180 datasets were labeled artificial. Conversely, **WGA** reads with structures validated in
181 one or more bulk datasets were labeled biological.

182 Application of this labeling strategy to the PC3 **WGA** data (Extended Table 1)
183 quantified the read distribution across these categories (Extended Data Fig. 1). We
184 identified 12,670,396 chimeric reads with zero matches in the bulk reference, which

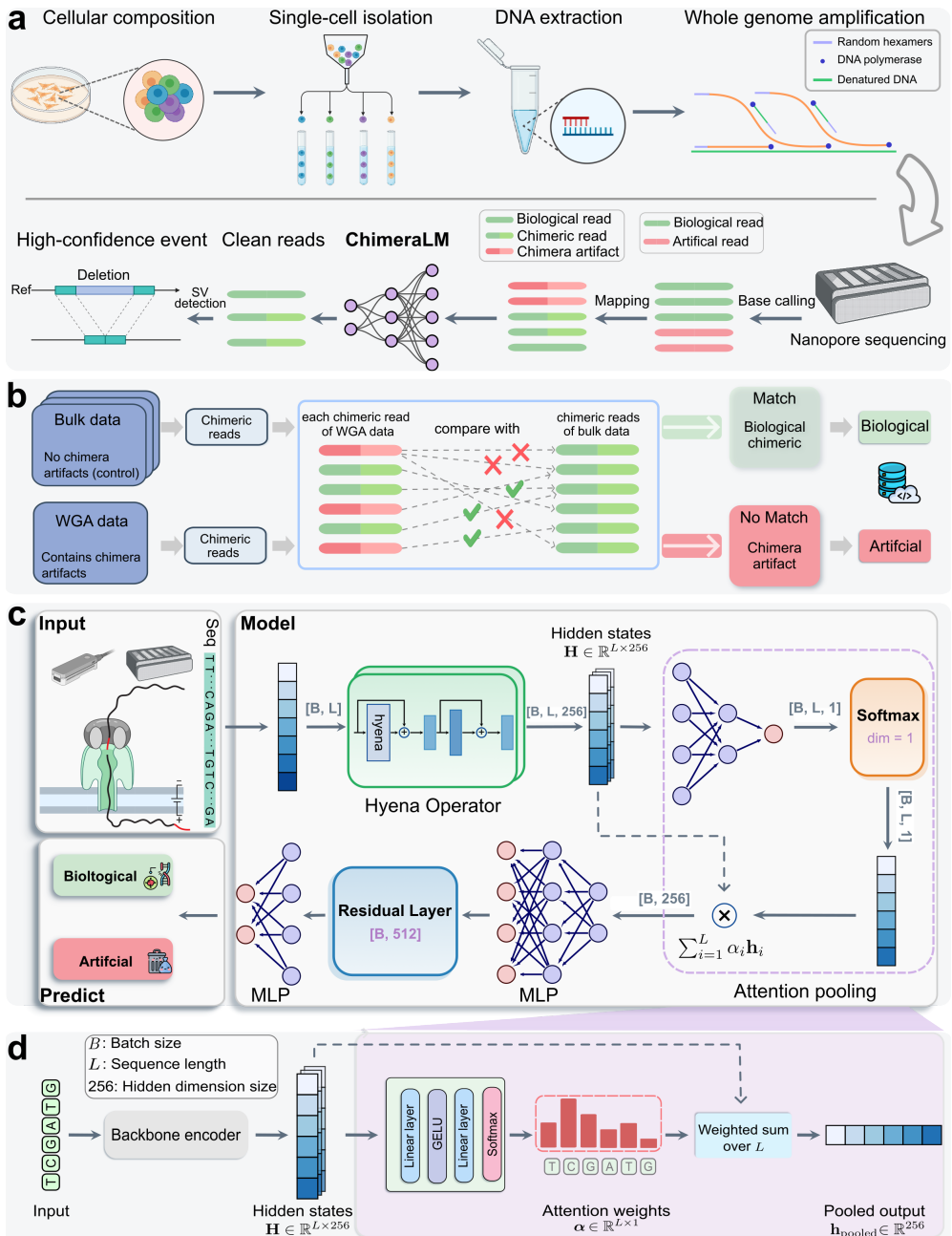


Fig. 1 ChimeraLM workflow and architecture for detecting WGA artifacts in single-cell sequencing. (a) Single-cell genomic workflow and ChimeraLM integration. Single cells are isolated, followed by DNA extraction and WGA for genome amplification. WGA generates chimeric artifacts (red) through template switching during amplification, alongside biological reads (green). After nanopore sequencing, ChimeraLM classifies chimeric reads as biological or artificial, enabling downstream SV detection on clean reads. (b) Ground truth label generation for supervised learning. Chimeric reads from WGA data are compared against all chimeric reads from bulk sequencing data of the same cell line. Reads that match bulk data are labeled as biological (green pathway), while non-matching reads are labeled as chimera artifacts (red pathway). This provides reliable training labels. (c) ChimeraLM architecture. Input DNA sequences (batch size B , sequence length L) are tokenized and encoded into hidden states $H \in \mathbb{R}^{L \times 256}$ through a backbone encoder (HyenaDNA [?]). Hyena operators capture long-range dependencies in genomic sequences. Attention pooling aggregates position-specific features using learned weights. Residual and multilayer perceptron (MLP) layers process pooled features, and a softmax layer outputs binary classification probabilities for biological versus artificial reads. (d) Attention pooling mechanism detail. The backbone encoder (HyenaDNA) transforms input sequences into hidden state $H \in \mathbb{R}^{L \times 256}$. Attention weights $\alpha \in \mathbb{R}^{L \times 1}$ are computed through linear layers, GELU activation, and softmax normalization, assigning importance scores to each nucleotide position. The weighted sum $h_{\text{pooled}} = \sum_{i=1}^L \alpha_i h_i$ produces the pooled output $h_{\text{pooled}} \in \mathbb{R}^{256}$, compressing variable-length sequences into fixed-dimensional representations. Created with BioRender.com.

231 were classified as artificial. Conversely, we identified a total of 293,180 reads validated
232 as biological. This biological set was composed of reads matching one (Match 1: 101,094
233 reads), two (Match 2: 190,309 reads), or all three (Match 3: 1,777 reads) of the bulk
234 reference datasets. To construct a balanced training dataset, we retained all 293,180
235 biological reads (combining Match 1, 2, and 3) and subsampled an equal number
236 (293,180) of artificial reads from the no-match category. This set was augmented with
237 178,748 chimeric reads subsampled from the bulk datasets as positive controls. The
238 final dataset of 765,108 labeled reads was partitioned into training (70%), validation
239 (20%), and internal test (10%) sets using stratified splitting.

240 The architecture of ChimeraLM (Fig. 1c) was specifically designed to learn from
241 this dataset by operating directly on raw DNA sequences, bypassing conventional,
242 feature-based classifiers. This design must address three primary technical chal-
243 lenges: (1) efficiently processing variable-length sequences of many kilobases, and
244 (2) simultaneously maintaining single-nucleotide resolution to detect the precise,
245 abrupt compositional changes that define chimeric junctions, and (3) aggregating
246 variable-length sequence representations into a consistent classification output.

247 ChimeraLM first addresses the need for high resolution by tokenizing input
248 sequences at the single-nucleotide level. This base-pair precision is required to preserve
249 the complete sequence information necessary for detecting chimeric junctions—the
250 breakpoints where disparate genomic regions are artificially fused and which often
251 exhibit abrupt compositional changes.

252 The architecture’s core employs Hyena operators [?], selected specifically to
253 overcome the challenge of processing long DNA sequences. Traditional attention
254 mechanisms scale quadratically with sequence length, making them computationally
255 prohibitive for long-read data. Hyena operators, by contrast, achieve subquadratic
256 scaling, enabling ChimeraLM to analyze full-length reads without fragmentation and
257 thus preserve the structural context around chimeric junctions. To leverage existing
258 genomic knowledge, we initialized the model with weights from HyenaDNA [?], a
259 genomic foundation model pre-trained on diverse DNA sequences.

260 Finally, to produce a classification, the model employs an attention pooling mech-
261 anism to aggregate information across the entire variable-length read (Fig. 1d). This
262 module computes learned, position-specific weights to identify which nucleotides—such
263 as those at the junction boundary—are most informative for the classification deci-
264 sion. This weighted aggregation produces a fixed-dimensional representation, which
265 is then processed through MLP components with residual connections. A final soft-
266 max layer outputs the probability scores for the biological versus artificial classes (see
267 Methods). This end-to-end architecture enables ChimeraLM to learn directly from
268 raw sequence data, discovering complex patterns that may not be apparent through
269 rule-based algorithms.

270

271 **ChimeraLM achieves high accuracy and reduces artifacts to 272 near-bulk levels across platforms**

273

274 We first evaluated ChimeraLM’s classification accuracy on the held-out test set
275 (derived from the PromethION training data), which comprised reads with known bio-
276 logical or artificial status (Fig. 2a). The model achieved an F1 score of 0.81, reflecting

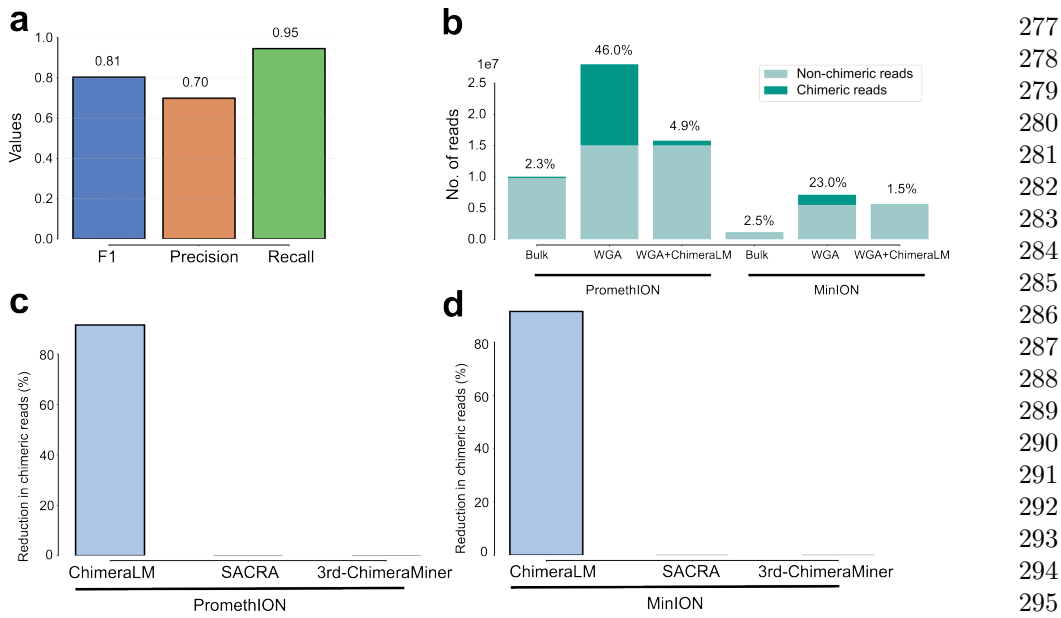


Fig. 2 ChimeraLM accurately identifies and removes WGA-induced chimeric artifacts.

(a) Classification performance on held-out test data. ChimeraLM achieves high recall (0.95) in identifying chimera artifacts while maintaining acceptable precision (0.70), yielding an F1 score of 0.81 for binary classification of biological versus artificial sequences. (b) Chimeric read reduction across sequencing platforms. Stacked bars show the proportion of chimeric (dark teal) and non-chimeric (light teal) reads in bulk sequencing, WGA-amplified samples, and ChimeraLM-filtered WGA samples. Data from PC3 cell line sequenced on PromethION (left) and MinION (right) platforms demonstrate that ChimeraLM reduces chimeric read frequencies from 46.0% to 4.9% (PromethION) and from 23.0% to 1.5% (MinION), approaching bulk levels (2.3% and 2.5%, respectively). (c,d) Benchmarking against existing methods. ChimeraLM achieves approximately 90% reduction in chimeric reads on both PromethION (c) and MinION (d) platforms, whereas existing computational tools SACRA and 3rd-ChimeraMiner show no detectable reduction in chimeric content.

balanced sensitivity and specificity in artifact detection. A recall of 0.95 indicates that 95% of true chimeric reads were correctly identified—critical for minimizing downstream false-positive structural variant calls—while a precision of 0.70 shows that the majority of reads flagged as chimeric were true artifacts. These results establish the model’s reliability for identifying amplification-induced artifacts in long-read data.

We next assessed its practical effectiveness on the full PC3 WGA datasets, comparing performance on the PromethION and MinION platforms (Fig. 2b). Bulk sequencing established a low baseline chimeric read rate (2.3% for PromethION; 2.5% for MinION). WGA dramatically increased this artifact load to 46.0% (PromethION) and 23.0% (MinION). After ChimeraLM filtering, chimeric content dropped to 4.9% on PromethION and 1.5% on MinION—representing 10- to 15-fold reductions—while retaining 15.8 million and 5.6 million biological reads. This restoration to near-bulk quality demonstrates that ChimeraLM effectively separates genuine genomic reads from WGA-induced artifacts.

277
278
279
280
281
282
283
284
285
286
287
288
289
290
291
292
293
294
295
296
297
298
299
300
301
302
303
304
305
306
307
308
309
310
311
312
313
314
315
316
317
318
319
320
321
322

323 We then benchmarked ChimeraLM against existing computational tools for detect-
324 ing amplification-induced chimeras, SACRA [?] and 3rd-ChimeraMiner [?] (Fig. 2c,d).
325 When applied to the same PromethION and MinION **WGA** data, ChimeraLM
326 achieved an approximately 90% reduction in chimeric reads on both platforms. In stark
327 contrast, neither SACRA nor 3rd-ChimeraMiner showed any detectable reduction in
328 chimeric content (0% reduction).

329 Together, these results demonstrate a robust and generalizable performance. The
330 strong filtering on the MinION dataset (Fig. 2b) is particularly noteworthy, as this
331 dataset served as a completely independent test set; the model was trained exclu-
332 sively on PromethION data. This cross-platform generalization, combined with the
333 high recall on the internal test set (Fig. 2a) and the clear superiority over existing tools
334 (Fig. 2c,d), indicates that ChimeraLM learns fundamental, generalizable sequence
335 features of **WGA**-induced artifacts rather than platform-specific signatures.

336

337

338

339

340

341

342

343

344

345

346

347

348

349

350

351

352

353

354

355

356

357

358

359

360

361

362

363

364

365

366

367

368

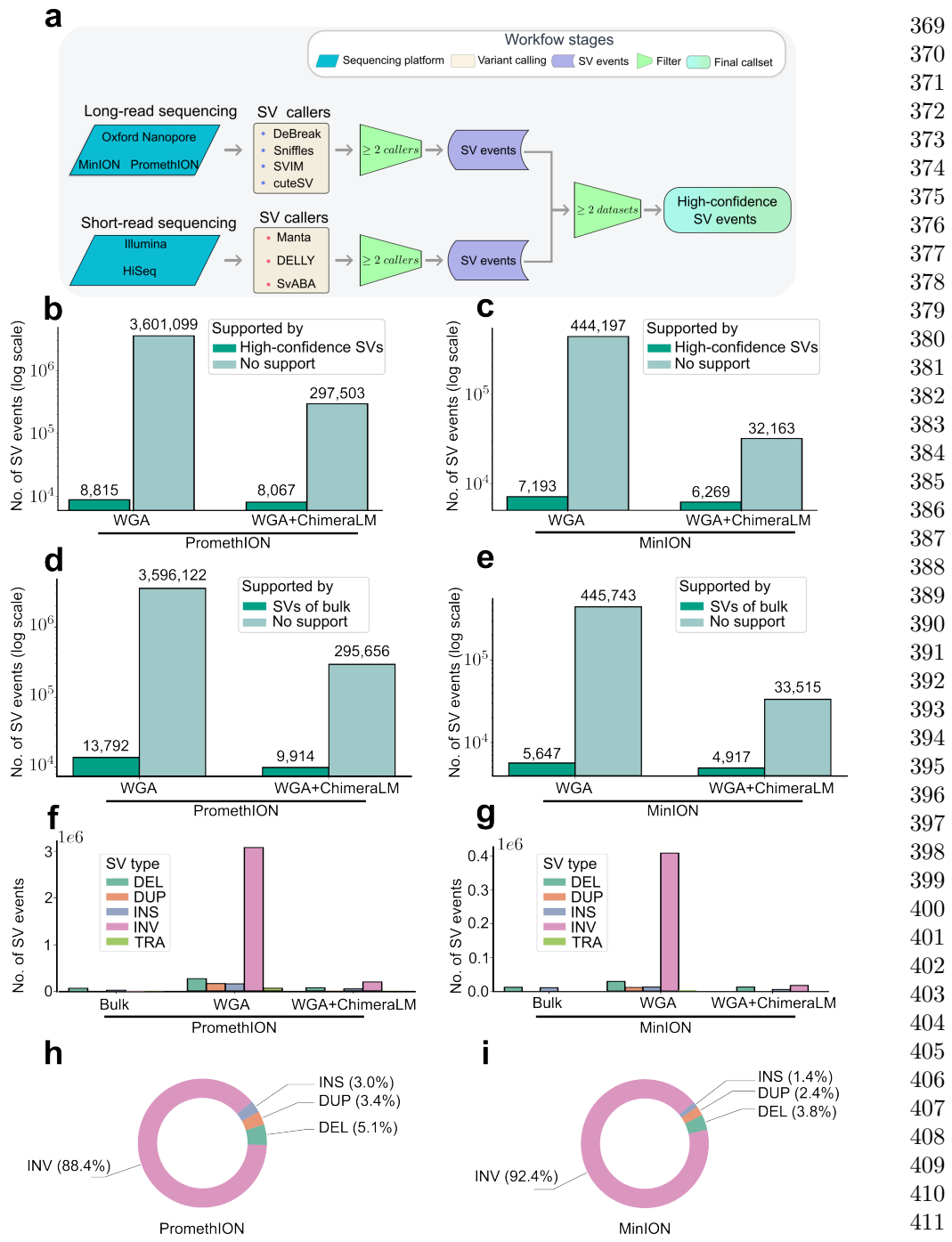


Fig. 3 ChimeraLM improves structural variant detection accuracy. (a) Construction of high-confidence SV reference dataset. PC3 bulk DNA was sequenced on multiple platforms (ONT PromethION and MinION, Illumina HiSeq) and analyzed with multiple SV calling algorithms. SV events detected by ≥2 callers on the same platform were retained. Events supported by both long-read and short-read platforms were designated as high-confidence gold standard SVs. (b,c) SV validation against multi-platform gold standard. Stacked bars show total SV calls (log scale, numbers above bars) classified as gold standard-supported (dark teal) or unsupported (light teal) for PromethION (b) and MinION (c). ChimeraLM substantially reduces unsupported SV calls while preserving gold standard events. (d,e) SV validation against long-read bulk sequencing (ONT PromethION and MinION). Stacked bars show SV calls classified as bulk-supported (dark teal) or unsupported (light teal) for PromethION (d) and MinION (e). Long-read bulk data from the same platform provides platform-matched validation, capturing true variants that may be specific to long-read detection. (f,g) SV type distribution across processing methods. Bar charts show the number of detected SVs by type: DEL (green), duplication (DUP) (orange), INS (blue), INV (pink), and TRA (light green) for PromethION (f) and MinION (g). Unfiltered WGA data shows elevated counts across all types, particularly INVs and TRAs, which are reduced to bulk-like levels after ChimeraLM filtering. (h,i) Composition of chimeric artifact-supported SVs. Pie charts show the proportion of SV types among events supported exclusively by reads classified as chimeric artifacts in unfiltered WGA data for PromethION (h) and MinION (i). These represent false-positive SV calls that would be eliminated by ChimeraLM.

415 **ChimeraLM substantially reduces false-positive structural
416 variant calls**

417 Accurate **SV** detection is essential for understanding genomic diversity and dis-
418 ease mechanisms in single cells. However, **WGA**-induced chimeric artifacts can be
419 misidentified as genuine **SVs**, leading to incorrect biological conclusions. To quantify
420 ChimeraLM’s impact on **SV** calling accuracy, we compared variant calls from unfiltered
421 **WGA** data and ChimeraLM-filtered data against two independent reference standards
422 (Fig. 3).

423 We first established a high-confidence gold standard **SV** dataset by integrating
424 results from bulk PC3 DNA sequenced on multiple platforms (**ONT** PromethION,
425 **ONT** MinION, and Illumina HiSeq) and analyzed with multiple **SV** callers (Fig. 3a;
426 Extended Table 1). **SVs** detected by ≥ 2 callers on the same platform and supported
427 by both long-read and short-read data were retained as gold-standard events, ensuring
428 high specificity across technologies.

429 Comparison against this gold standard revealed that unfiltered **WGA** data con-
430 tained extensive false-positive **SVs** (Fig. 3b,c). On PromethION, raw **WGA** data
431 produced 3.6 million **SV** calls, of which only 8,815 (0.24%) matched gold standard
432 events—indicating that over 99% were artifacts. After ChimeraLM filtering, total calls
433 dropped to 305,570 while retaining 8,067 true events, raising the validation rate to
434 2.64% (11-fold improvement) and preserving 91.5% of true variants. MinION data
435 showed similar results, with calls reduced from 451,390 to 38,432 and the validation
436 rate increasing from 1.59% to 16.3% (10-fold improvement) while retaining 87.2% of
437 true variants. These results highlight ChimeraLM’s ability to remove spurious **SV** calls
438 while maintaining biological sensitivity.

439 To complement this stringent validation, we next performed platform-matched bulk
440 validation, comparing **WGA**-derived **SV** calls against long-read bulk sequencing from
441 the same platform (Fig. 3d,e). This reference captures true **SVs** that may be missed by
442 short-read data, providing a more inclusive measure of recall. Under this benchmark,
443 ChimeraLM increased validation rates from 0.38% to 3.24% on PromethION (8.5-
444 fold improvement) and from 1.25% to 12.79% on MinION (10-fold improvement),
445 while retaining 71.9% and 87.1% of bulk-supported events, respectively. The consistent
446 improvements across independent datasets demonstrate that ChimeraLM effectively
447 suppresses **WGA**-induced artifacts without sacrificing detection of genuine **SVs**.

448 Together, these analyses demonstrate that ChimeraLM reduces false-positive **SV**
449 calls by 8–16 fold while preserving 72–92% of true variants, resulting in a substantial
450 enhancement of the signal-to-noise ratio in single-cell **SV** discovery. By restoring near-
451 bulk specificity and maintaining robust sensitivity, ChimeraLM enables more accurate
452 and interpretable downstream genomic analyses.

453
454 **ChimeraLM restores unbiased SV-type distributions and
455 characterizes artifact composition**

456 Amplification artifacts can distort the apparent spectrum of **SVs**, often inflating spe-
457 cific **SV** types. To evaluate whether ChimeraLM effectively corrects such distortions,
458
459
460

we compared **SV** type distributions across bulk, unfiltered **WGA**, and ChimeraLM-filtered datasets (Fig. 3f,g). Bulk sequencing showed relatively balanced proportions of **DELs**, **DUPs**, **INSSs**, **INVs**, and **TRAs**. In contrast, unfiltered **WGA** data exhibited a dramatic overrepresentation of **INVs** on both PromethION and MinION platforms, consistent with pervasive amplification artifacts. After ChimeraLM filtering, these distributions were largely restored toward bulk-like profiles: excessive **INVs** were markedly reduced while other **SV** categories remained stable. This shift reflects selective removal of artifact-supported **INVs** rather than indiscriminate loss of genuine inversion signals, demonstrating high specificity in distinguishing chimeric from biological reads.

To investigate the basis of this normalization, we analyzed **SV** calls supported exclusively by reads classified as chimeric by ChimeraLM (Fig. 3h,i). These artifact-supported events were overwhelmingly dominated by **INVs**, comprising 88.4% on PromethION and 92.4% on MinION. This pattern is consistent with template-switching junctions that produce inversion-like alignment signatures. Smaller fractions of **DELs** (5.1% and 3.8%), **DUPs** (3.4% and 2.4%), and **INSSs** (3.0% and 1.4%) were also observed, demonstrating that **WGA**-induced chimeras can mimic diverse **SV** categories rather than only **INVs**.

This characterization has important implications for single-cell genomics. Although **INVs** are the predominant artifact type, the coexistence of **DELs**, **DUPs**, and **INSSs** among chimeric events indicates that comprehensive filtering—rather than inversion-specific correction—is essential for accurate **SV** detection. Without ChimeraLM filtering, single-cell **SV** analyses would be confounded not only by false-positive **INVs** but also by other artifact-associated variants [? ?]. By restoring biologically representative **SV** type distributions, ChimeraLM enables robust and interpretable characterization of structural variation in single cells without distortion from **WGA**-induced artifacts.

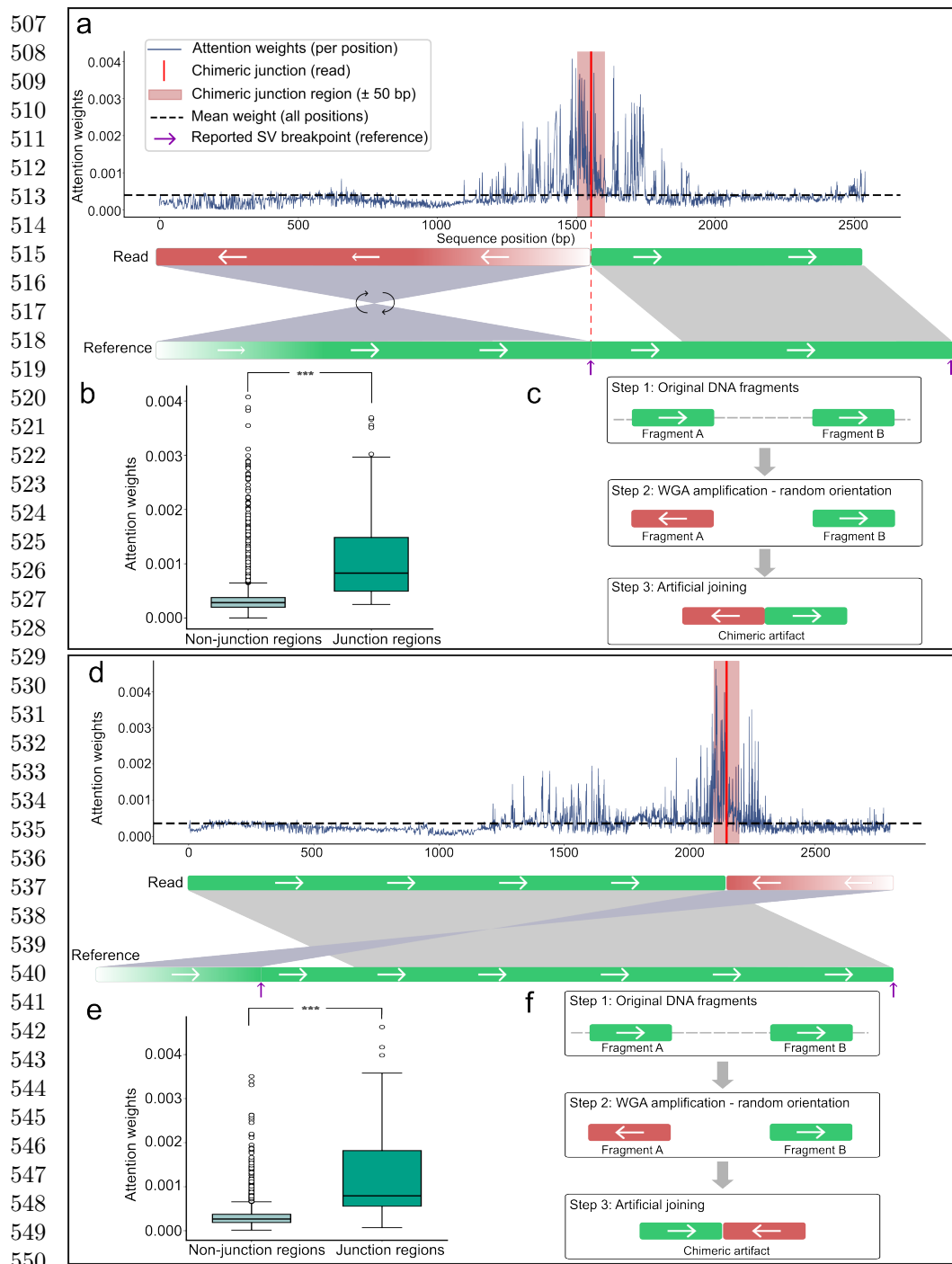


Fig. 4 ChimeraLM attention weights can localize to chimeric junction regions.

(a,d) Attention weight profiles for two representative chimeric reads. Upper panels show attention weights per sequence position (blue line) and mean attention (dashed line). Red vertical lines mark chimeric junction positions, with pink shading indicating junction region (± 50 bp). Purple arrows show reported SV breakpoints. Lower panels illustrate read alignments: reads (top bars) show orientation transitions at junctions (green = forward, red = reverse-complemented, arrows indicate strand), while reference genome (bottom bars) maintains continuous forward orientation. Gray regions connect aligned segments. (b,e) Quantitative attention analysis. Box plots show significantly elevated attention weights in junction region versus non-junction regions for both examples ($p = 5.3 \times 10^{-14}$ and $p = 6.8 \times 10^{-15}$, respectively; Wilcoxon rank-sum test). (c,f) Proposed chimera formation mechanisms. Step 1: Original DNA fragments from distant genomic loci exist in forward orientation. Step 2: During WGA, one or both fragments may undergo random reverse-complementation. Step 3: Template switching joins the fragments with discordant orientations, creating chimeric artifacts. The two examples illustrate different orientation patterns (forward-to-reverse vs reverse-to-forward transitions) arising from random strand selection during amplification.

ChimeraLM provides interpretable classification through attention visualization	553
	554
	555
	556
	557
	558
	559
	560
	561
	562
	563
	564
	565
	566
	567
We next investigated whether ChimeraLM’s attention mechanism highlights biologically meaningful regions within sequencing reads (Fig. 4). For representative chimeric reads, attention weight profiles showed low baseline values across most positions but pronounced peaks at junction regions where template switching artificially joins DNA fragments from distinct genomic loci (Fig. 4a,d). These peaks coincided precisely with alignment breakpoints characterized by orientation changes between adjacent read segments—the defining signature of WGA-induced chimeric artifacts.	568
Quantitative analysis confirmed that attention weights within junction regions (± 50 bp) were significantly higher than those in non-junction regions (Wilcoxon rank-sum test, $p = 5.3 \times 10^{-14}$ and $p = 6.8 \times 10^{-15}$) (Fig. 4b,e). Such localization indicates that ChimeraLM learns mechanistically relevant features associated with artificial junction formation rather than relying on spurious correlations.	569
Schematic reconstruction of the amplification process further supports this interpretation (Fig. 4c,f). During WGA, DNA fragments from distant genomic loci may undergo random strand orientation changes before being joined by template switching. This process produces artificial junctions with discordant orientations—forward-to-reverse or reverse-to-forward—that generate inversion-like alignment signatures and are effectively recognized by the model’s attention peaks.	570
Together, these analyses demonstrate that ChimeraLM’s attention mechanism can localize chimeric junctions at single-base resolution and capture the underlying orientation discontinuities that define WGA-induced artifacts.	571
	572
	573
	574
	575
	576
	577
	578
	579
	580
	581
	582
	583
	584
	585
	586
	587
	588
	589
	590
	591
	592
	593
	594
	595
	596
	597
	598
Discussion	577
WGA has enabled genomic analysis from single cells but introduces chimeric artifacts that compromise SV detection. ChimeraLM addresses this challenge through sequence-level classification of biological versus artificial reads, substantially improving SV calling accuracy before downstream analysis. This upstream filtering strategy—removing problematic sequences at the read level rather than correcting errors post hoc—provides a practical solution for single-cell genomics laboratories.	578
Our results demonstrate several key advantages of ChimeraLM for long-read single-cell sequencing. The method achieves approximately 90% reduction in chimeric reads across nanopore platforms while retaining 87–92% of true SVs. It reduces false-positive SV calls by 8–16 fold, enabling researchers to focus on biologically relevant variants without manually filtering thousands of artifacts. Moreover, ChimeraLM performs consistently across PromethION and MinION without platform-specific retraining, indicating that it captures generalizable sequence features of WGA-induced chimeras. These results underscore the model’s robustness across diverse datasets and sequencing conditions.	579
ChimeraLM’s effectiveness reflects the ability of deep learning models to capture complex sequence patterns that are difficult to encode in rule-based filters. Traditional quality control methods rely on predefined metrics such as mapping quality or read	580

599 depth [? ?], which may not effectively distinguish chimeric artifacts from biological reads. By learning directly from data, ChimeraLM discovers subtle compositional
600 and structural features that differentiate authentic genomic sequences from amplification artifacts. Furthermore, the model offers interpretability through attention
601 visualization, allowing researchers to examine which sequence regions drive classification.
602 Attention weights can concentrate sharply at junctions where template switching
603 joins DNA fragments from distinct loci, matching the known mechanism of chimera
604 formation. Some reads show more diffuse attention distributions, suggesting that
605 ChimeraLM integrates multiple complementary cues—such as junction orientation,
606 compositional biases, and local sequence context—to classify diverse artifact types.
607 This interpretability builds confidence in the model’s predictions and provides a lens
608 for probing the molecular processes underlying amplification-induced artifacts.

611 The improved reliability of **SV** detection has direct implications for single-cell
612 genomics. Studies of chromosomal instability, clonal evolution, and **SV** burden in individual
613 cells have long been constrained by high false-positive rates in **WGA** data [? ?].
614 ChimeraLM enables more confident identification of genuine **SVs**, supporting
615 research in cancer genomics, developmental biology, and aging where single-cell resolution
616 is essential for understanding cellular heterogeneity. Although the current model
617 processes reads independently, integrating additional contextual features—such as coverage,
618 mate-pair, or phasing information—could further enhance accuracy. **Graphics Processing Unit (GPU)**
619 resources are recommended for large-scale datasets, while **Central Processing Unit (CPU)** inference remains feasible for smaller studies; runtime
620 optimization and model compression may improve accessibility for broader use.

622 Future work should prioritize validation across diverse biological contexts in
623 long-read single-cell sequencing. Testing on multiple cell types (primary, stem, or
624 immune cells) and **WGA** protocols will establish generalizability. The interpretability
625 of attention-based models could also be leveraged to investigate mechanisms of
626 chimera formation: large-scale analysis of attention patterns may reveal recurrent
627 sequence motifs or genomic contexts associated with template switching, guiding the
628 development of improved amplification protocols. More broadly, ChimeraLM illus-
629 trates the potential of **GLMs** for data quality control applications [?]. Architectural
630 innovations such as the Hyena operator for efficient long-range modeling [?] may
631 have utility beyond chimera detection, addressing challenges such as contamination,
632 adapter artifacts, and systematic sequencing errors.

633 ChimeraLM thus provides a practical and interpretable framework for improving
634 long-read single-cell genomic data quality. By removing **WGA**-induced chimeric arti-
635 facts at the read level and revealing the mechanistic features that drive them, the
636 method not only enhances **SV** detection reliability but also deepens understanding of
637 amplification-induced bias in single-cell genomics.

638
639
640
641
642
643
644

Methods	645
Cell culture, single-clone preparation, and nanopore sequencing	646
<i>Cell culture and single-clone establishment</i>	647
PC3 prostate cancer cells (ATCC® CRL-1435™) were cultured in RPMI-1640 medium supplemented with 10% fetal bovine serum and 1% penicillin–streptomycin at 37 °C with 5% CO ₂ . To minimize biological heterogeneity, a monoclonal population was established by serial dilution in 96-well plates, ensuring that each culture originated from a single cell. Mycoplasma contamination was routinely tested and confirmed negative prior to DNA extraction.	648 649 650 651 652 653 654 655 656 657
<i>DNA extraction and whole-genome amplification</i>	658
From the monoclonal population, two types of DNA samples were prepared: a bulk (non-amplified) control and ten single-cell MDA-amplified genomes. Bulk high-molecular-weight DNA was extracted using the Monarch® HMW DNA Extraction Kit for Cells & Blood (New England Biolabs). Individual cells were isolated using 1CellDish-60 mm (iBiochips) and amplified using the REPLI-g Advanced DNA Single Cell Kit (Qiagen) following the manufacturer's protocol. DNA concentration and fragment integrity were assessed with a Qubit 4 fluorometer and Agilent TapeStation (DNA 1000/5000 ScreenTape). Only samples meeting quality standards were used for library construction.	659 660 661 662 663 664 665 666 667
<i>Nanopore library preparation and sequencing</i>	668
Sequencing libraries were prepared using the ONT Ligation Sequencing Kit V14 (SQK-LSK114) and sequenced on MinION Mk1C or PromethION P2 Solo devices with R10.4.1 flow cells according to the manufacturer's genomic DNA workflow. Because all single-cell samples originated from the same monoclonal lineage, observed differences between amplified and bulk data primarily reflect MDA-induced artifacts rather than biological variation, providing a controlled experimental setting for downstream analyses.	669 670 671 672 673 674 675 676 677 678
<i>Basecalling and read processing</i>	679
Raw signal files (POD5) were basecalled using Dorado v0.5.0 with the high-accuracy model <code>dna_r10.4.1_e8.2_400bps_hac@v4.3.0</code> [?]. Reads with mean quality < 10 or length < 500 bp were removed. Residual adapters and concatemers were trimmed using Cutadapt v4.0 [?] in two-pass error-tolerant mode. Cleaned reads were aligned to the GRCh38.p13 reference genome using minimap2 v2.26 (<code>map-ont</code> preset) [?]. Resulting BAM files were sorted and indexed with SAMtools v1.16 [?]. Read length and mapping statistics were calculated using NanoPlot v1.46.1 [?]. All samples were processed under identical parameters to ensure consistency across datasets.	680 681 682 683 684 685 686 687 688 689 690
<i>Chimeric read identification</i>	687
Chimeric reads were identified based on the presence of supplementary alignments in BAM files using the Supplementary Alignment (SA) tag. The <code>SA</code> tag indicates that	688 689 690

691 a read has additional alignments beyond the primary alignment, which is character-
692 istic of chimeric sequences that map to multiple distant genomic locations. To ensure
693 accurate identification, we applied stringent filtering criteria: reads were classified as
694 chimeric only if they (1) were not unmapped, (2) contained the **SA** tag, (3) were not
695 secondary alignments, and (4) were not supplementary alignments themselves. This
696 filtering approach ensures that only primary alignments with supplementary mapping
697 evidence are considered chimeric, avoiding double-counting of the same chimeric event
698 and excluding low-quality or ambiguous alignments. Reads without the **SA** tag (single
699 continuous alignments) were classified as non-chimeric. This approach leverages the
700 standard BAM format specification to reliably identify reads with complex alignment
701 patterns.

702

703 **Training data construction**

704

705 *Data generation and sources*

706 To construct the training dataset, we generated **WGA** and bulk sequencing data from
707 PC3 cells. The **WGA** sample was amplified and sequenced on the PromethION P2 plat-
708 form (**ONT**), while three independent bulk datasets were produced from non-amplified
709 genomic DNA: bulk PromethION P2, bulk MinION Mk1c (**ONT**), and bulk PacBio.
710 These bulk datasets represent authentic biological sequences free from amplification-
711 induced artifacts. In contrast, **WGA** sequencing includes both genuine genomic reads
712 and artificial chimeras introduced during the amplification process. An additional
713 **WGA** dataset sequenced on the MinION Mk1c platform was reserved exclusively as
714 an independent test set for cross-platform evaluation.

715

716 *Ground truth annotation and class definition*

717 Ground truth labels were established by systematically comparing chimeric reads from
718 the **WGA** PromethION P2 dataset against those from the three bulk datasets. For
719 each **WGA** chimeric read, all alignment segments—defined by their genomic start
720 and end coordinates—were compared to the corresponding segments of bulk chimeric
721 reads. A **WGA** read was labeled as biological if every segment matched at least one
722 bulk chimeric read within a 1 kb positional tolerance, indicating that the structural
723 configuration is also present in non-amplified DNA. Reads lacking any matching pat-
724 tern across all bulk datasets were labeled as artificial chimeras, presumed to arise
725 from the amplification process. To ensure balanced class representation, additional
726 chimeric reads were randomly sampled from the bulk datasets and labeled as biologi-
727 cal, as these reads originate from genuine genomic rearrangements such as true **SVs**.
728 The final labeled dataset combined the annotated **WGA** PromethION P2 reads with
729 the subsampled bulk chimeric reads and was subsequently partitioned into training,
730 validation, and test sets as described below.

731

732 *Dataset partitioning and cross-platform validation*

733 The combined labeled dataset, derived from **WGA** PromethION P2 and bulk sequenc-
734 ing data, was divided into training (70%), validation (20%), and internal test (10%)
735 sets using stratified random sampling to maintain class balance. These subsets
736

were used respectively for model training, hyperparameter tuning, and performance evaluation on data from the same sequencing platform. 737
738

To evaluate cross-platform generalization, the complete WGA MinION Mk1c dataset was reserved as an independent external test set. This dataset, generated on a different nanopore platform, was never used during model training or internal testing. This two-level evaluation design allowed us to test whether ChimeraLM captures general sequence features of amplification-induced chimeras rather than platform-specific artifacts. 739
740
741
742
743
744
745

Model architecture 746

Backbone encoder 747

ChimeraLM employs the pre-trained HyenaDNA model [?] as its backbone encoder. This model was pre-trained on large-scale genomic data and provides robust sequence representations. DNA sequences are tokenized at single-nucleotide resolution, with each base (A, C, G, T, N) mapped to a unique integer token (7, 8, 9, 10, 11, respectively). Special tokens include [CLS]=0, [PAD]=4, and others for sequence processing. Input sequences are truncated at 32,768 bp or padded to enable batch processing. 748
749
750
751
752
753
754

For a tokenized input sequence $\mathbf{x} \in \mathbb{Z}^L$, the HyenaDNA backbone generates contextualized hidden representations: 755
756
757

$$\mathbf{H} = \text{HyenaDNA}(\mathbf{x}) \in \mathbb{R}^{L \times 256}$$

where $\mathbf{H} = (\mathbf{h}_1, \mathbf{h}_2, \dots, \mathbf{h}_L)$ represents position-wise hidden states with dimension 256. The Hyena operators [?] efficiently capture both local sequence motifs and long-range dependencies essential for distinguishing biological sequences from chimeric artifacts. 759
760
761
762
763
764

Attention pooling 765

To aggregate variable-length sequence representations into fixed-size vectors, ChimeraLM implements attention-based pooling. For hidden states $\mathbf{H} \in \mathbb{R}^{L \times 256}$, attention weights are computed through a two-layer network: 766
767
768
769
770
771
772
773
774
775
776
777
778
779
780
781
782

The pooled representation is the weighted sum of hidden states:

$$\mathbf{h}_{\text{pooled}} = \sum_{i=1}^L \alpha_i \mathbf{h}_i \in \mathbb{R}^{256}$$

This mechanism assigns learned importance weights to each sequence position, enabling the model to focus on informative regions while accommodating natural variability in read lengths.

783 ***Classification head***
 784 The pooled representation is processed through a **MLP** with residual connections. The
 785 first layer expands dimensionality:
 786

$$787 \quad \mathbf{f}_1 = \text{Dropout}_{0.1}(\text{GELU}(\text{Linear}_{256 \rightarrow 512}(\mathbf{h}_{\text{pooled}}))) \in \mathbb{R}^{512}$$

788
 789 Subsequent residual blocks with input $\mathbf{f}_{\text{in}} \in \mathbb{R}^{512}$ compute:
 790

$$791 \quad \mathbf{f}_{\text{out}} = \text{Dropout}_{0.1}(\text{Linear}_{512 \rightarrow 512}(\text{GELU}(\text{Linear}_{512 \rightarrow 512}(\mathbf{f}_{\text{in}})))) + \mathbf{f}_{\text{in}}$$

792 where the skip connection enables stable gradient flow during training. The final layer
 793 produces binary classification logits:
 794

$$795 \quad \mathbf{z} = [z_0, z_1] = \text{Linear}_{512 \rightarrow 2}(\mathbf{f}_{\text{final}}) \in \mathbb{R}^2$$

796 where z_0 and z_1 represent logits for biological and artificial chimeric classes, respec-
 797 tively. During inference, the predicted class is $\hat{y} = \text{argmax}_{i \in \{0,1\}} z_i$.
 800

801 ***Model summary***
 802 The complete ChimeraLM pipeline processes DNA sequences through: (1) single-
 803 nucleotide tokenization, (2) HyenaDNA backbone encoding to generate contextualized
 804 representations, (3) attention pooling to aggregate position-specific features, (4) **MLP**
 805 layers with residual connections to learn classification features, and (5) binary classi-
 806 fication output. The entire model is trained end-to-end using labeled **WGA** and bulk
 807 sequencing data.
 808

809 ***Model training and optimization***
 810

811 ***Training configuration***
 812 ChimeraLM was trained using PyTorch [?] and PyTorch Lightning [?] frameworks.
 813 Input sequences were tokenized using the tokenizer with maximum sequence length of
 814 32,768 bp. Sequences longer than this threshold were truncated; shorter sequences were
 815 padded to enable batch processing. Training employed mixed-precision computation
 816 (bf16) to accelerate training while maintaining numerical stability.
 817

818 ***Optimization procedure***
 819 We used the AdamW optimizer [?] with learning rate 1×10^{-4} and weight decay
 820 0.01. A ReduceLROnPlateau scheduler dynamically adjusted the learning rate based
 821 on validation loss, reducing it by a factor of 0.1 when no improvement occurred for 10
 822 consecutive epochs. Early stopping with patience of 10 epochs prevented overfitting
 823 by terminating training when validation performance plateaued. A fixed random seed
 824 (12345) ensured reproducibility across training runs.
 825 The training objective used cross-entropy loss for binary classification. For a train-
 826 ing example with true class label $y \in \{0, 1\}$ and model logits $z = [z_0, z_1]$, the loss
 827

828

is:	829
$\mathcal{L} = -\log \left(\frac{\exp(z_y)}{\exp(z_0) + \exp(z_1)} \right)$	830
where z_0 and z_1 represent logits for biological and artificial chimeric classes.	831
Training implementation	832
Training used batch size of 16 sequences with 30 parallel data loading workers. GPU acceleration was employed for efficient processing, with training typically requiring 96-120 hours depending on dataset size. Model checkpointing saved the best-performing model based on validation metrics. Configuration management used Hydra [?] to enable reproducible experimentation.	833
Model evaluation	834
Performance was monitored using accuracy, precision, recall, and F1 score on the validation set after each epoch:	835
$\text{Precision} = \frac{\text{TP}}{\text{TP} + \text{FP}}, \quad \text{Recall} = \frac{\text{TP}}{\text{TP} + \text{FN}}$	836
$\text{F1} = \frac{2 \times \text{Precision} \times \text{Recall}}{\text{Precision} + \text{Recall}}, \quad \text{Accuracy} = \frac{\text{TP} + \text{TN}}{\text{TP} + \text{TN} + \text{FP} + \text{FN}}$	837
where TP (true positives) are chimeric reads correctly classified as artificial, TN (true negatives) are biological reads correctly classified as biological, FP (false positives) are biological reads misclassified as artificial, and FN (false negatives) are chimeric reads misclassified as biological. Final model selection was based on best validation performance as determined by early stopping.	838
Model inference and application	839
Inference pipeline	840
To apply ChimeraLM to new WGA sequencing data, the model takes a BAM file as input. Chimeric reads are identified using SA tags and filtered to exclude unmapped, secondary, or supplementary alignments. Each chimeric read sequence is tokenized using the tokenizer (maximum length 32,768 bp, with truncation or padding as needed). The trained model processes sequences in batches, generating two logits $[z_0, z_1]$ for each read corresponding to biological and artificial chimeric classes. Classification is determined by $\hat{y} = \text{argmax}(z_0, z_1)$. ChimeraLM outputs a filtered BAM file containing only reads classified as biological, which can be directly used for downstream analyses including SV calling.	841
Performance evaluation	842
Test set evaluation	843
Final model performance was evaluated on the held-out test set and the independent MinION Mk1c dataset. Metrics (precision, recall, F1 score, accuracy) were computed as described in the training section, where true positives represent chimeric reads	844

875 correctly classified as artificial and true negatives represent biological reads correctly
876 classified as biological.

877

878 *SV calling*

879 **SVs** were called using multiple tools to ensure comprehensive detection. For long-
880 read data (ONT PromethION P2 and MinION Mk1c), we used Sniffles v2.5 [? ?],
881 DeBreak v1.2 [?], SVIM v2.0.0 [?], and cuteSV v2.1.1 [?]. For short-read data of the
882 PC3 cell line, we used both the CCLE Illumina whole-genome sequencing dataset and
883 the PRJNA361315 Illumina WGS dataset, processed with Manta v1.6.0 [?], DELLY
884 v1.5.0 [?], and SvABA v1.1.0 [?]. All tools were executed with default recommended
885 parameters.

886

887 *Gold standard SV dataset construction*

888 A high-confidence gold standard **SV** dataset was generated from bulk PC3 sequencing
889 data to evaluate the impact of ChimeraLM on **SV** detection accuracy (Fig. 3a). All
890 **SV** comparison and breakpoint correction were performed using OctopuSV v0.2.3 [?].
891 We used four datasets: bulk MinION Mk1c, bulk PromethION P2, the CCLE Illumina
892 WGS dataset, and the PRJNA361315 Illumina WGS dataset. Within each dataset, **SV**
893 events supported by at least two independent callers were retained. Variants supported
894 by two or more datasets were designated as gold standard **SVs** for benchmarking.
895

896

897 *SV benchmarking analysis*

898 To assess the impact of ChimeraLM on **SV** calling accuracy, we compared **SV** calls from
899 unfiltered **WGA** data and ChimeraLM-filtered **WGA** data against two references: (1)
900 the stringent multi-platform gold standard dataset, and (2) platform-matched long-
901 read bulk sequencing data. Benchmarking was performed using Truvari v4.2.2 [?]
902 with default parameters. **SVs** were considered supported if they matched reference
903 variants within the defined breakpoint tolerance. Validation rates were calculated as
904 the proportion of called **SVs** supported by the reference. This dual benchmarking
905 strategy quantifies both improvements in detecting high-confidence multi-platform
906 **SVs** and the retention of platform-specific true variants.

907

908 **Benchmarking against existing methods**

909 ChimeraLM was compared to two existing computational methods for detecting
910 amplification-induced chimeric artifacts: SACRA [?] (GitHub commit 9a2607e) and
911 3rd-ChimeraMiner [?] (GitHub commit 04b5233). Both tools were applied to **WGA**
912 data from PromethION P2 and MinION Mk1c platforms using default parameters as
913 recommended in their documentation. Performance was evaluated by measuring the
914 percentage reduction in chimeric reads relative to unprocessed **WGA** data. Chimeric
915 reads were identified using **WGA** tag-based alignment criteria (reads with **SA** tags
916 indicating split alignments), and reduction rates were calculated as the proportion of
917 chimeric reads removed by each method.

918

919

920

Attention weight analysis

To investigate ChimeraLM’s interpretability, we analyzed attention weights from the pooling mechanism for representative chimeric reads. Attention weights indicate the relative importance assigned to each sequence position during classification. For selected reads, we extracted per-position attention weights and visualized them alongside read alignments to identify whether the model focuses on mechanistically relevant regions.

Chimeric junction positions were identified from alignment data (defined by breakpoints in **SA** tags). A window of ± 50 bp surrounding each junction was designated as the junction region. Attention weights within junction region were compared to non-junction regions using the Wilcoxon rank-sum test [?], with statistical significance assessed at $p < 0.001$.

Data visualization

Figures were generated using Python with Matplotlib [?] and Seaborn [?].

Computing resources

Computations were performed on a **High Performance Computing (HPC)** server with 64-core Intel Xeon Gold 6338 CPU, 256 GB RAM, and two NVIDIA A100 **GPUs** (80 GB memory each).

Extended Data Table 1 Sequencing and alignment statistics of PC3

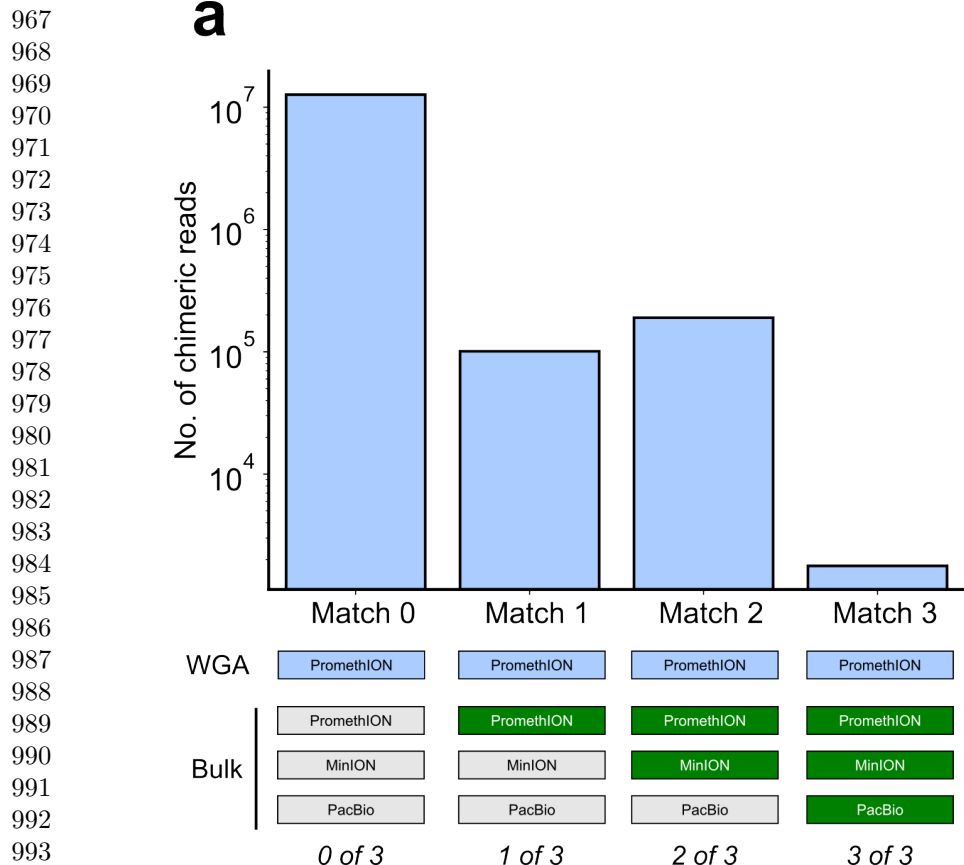
Sample	Platform	Reads ($\times 10^6$)	Total bases (Gb)	Total bases aligned (Gb)	Fraction aligned	Mean length (bp)	Mean quality (Q)	Average identity (%)
WGA	MinION	9.11	14.6	10.4	0.7	1,603	14.3	97.6
WGA	PromethION	44.69	128.2	69.2	0.5	2,869	14.5	96.1
Bulk	MinION	0.97	8.1	7.1	0.9	8,310	17.2	97.3
Bulk	PromethION	8.00	69.9	62.4	0.9	8,732	18.5	97.7

Supplementary information.

Acknowledgements. We thank Tingyou Wang for guidance on figure preparation. This project was supported in part by NIH grants R35GM142441 and R01CA259388 awarded to RY.

Declarations

Author Contributions. YL, QG and RY designed the study. YL and QG performed the analysis. QG performed the experiments. YL and QG designed and



995 **Extended Data Fig. 1. Distribution of chimeric read matches between WGA and bulk**
 996 **sequencing datasets.** Bar chart showing the number of chimeric reads (y-axis, log scale) grouped
 997 by how many bulk datasets (x-axis) contained matching chimeric structures when comparing WGA
 998 PromethION reads against bulk sequencing data. “Match 0” indicates reads with no matches in
 999 any bulk dataset (classified as artificial chimeras, $\sim 10^7$ reads), whereas “Match 1–3” indicate reads
 1000 with matches in one, two, or all three bulk datasets (classified as biological reads, $\sim 10^5$ reads each).
 1001 Symbols below the bars represent the number of bulk datasets with a match (0 of 3 – 3 of 3). This
 1002 matching scheme forms the basis for ground-truth labeling in supervised training.

1003 implemented the model. YL built the command-line tool and documentation. YL, QG
 1004 and RY wrote the manuscript. RY supervised this work.

1005 **Data Availability.** The raw sequencing data generated in this study have been
 1006 deposited in the NCBI Sequence Read Archive (SRA) under BioProject accession
 1007 PRJNA1354861. The dataset includes Oxford Nanopore long-read whole-genome
 1008 sequencing of PC3 prostate cancer cells and MDA-amplified single-cell derivatives. The
 1009 individual SRA accessions are as follows: PC3 bulk (MinION Mk1C), SRR35904028;
 1010 PC3 bulk (PromethION P2), SRR35904029; PC3 10-cell WGA (MinION Mk1C),
 1011 SRR35904026; PC3 10-cell WGA (PromethION P2), SRR35904027. We can access the
 1012

data at the following link: https://dataview.ncbi.nlm.nih.gov/object/PRJNA1354861? reviewer=viej6cv6mgbli3n7a9a5k1bsb3	1013
	1014
Code Availability. ChimeraLM, implemented in Python, is open source and available on GitHub (https://github.com/ylab-hi/ChimeraLM) under the Apache License, Version 2.0. The package can be installed via PyPI (https://pypi.org/project/chimeralm) using pip, with wheel distributions provided for Windows, Linux, and macOS to ensure easy cross-platform installation. For large-scale analyses, we recommend using ChimeraLM on systems with GPU acceleration. Detailed system requirements and optimization guidelines are available in the repository's documentation (https://ylab-hi.github.io/ChimeraLM/).	1015
	1016
	1017
	1018
	1019
	1020
	1021
	1022
	1023
	1024
	1025
	1026
	1027
	1028
	1029
CPU Central Processing Unit 15	1030
DEL deletion 3, 9, 11	1031
dMDA droplet-based MDA 2	1032
DOP-PCR Degenerate Oligonucleotide-Primed PCR 2	1033
DUP duplication 9, 11	1034
GLM Genomic Language Model 15	1035
GPU Graphics Processing Unit 15, 20, 22, 24	1036
HPC High Performance Computing 22	1037
INS insertion 3, 9, 11	1038
INV inversion 1, 3, 9, 11	1039
LIANTI Linear Amplification via Transposon Insertion 2, 14, 15	1040
MALBAC Multiple Annealing and Looping-based Amplification Cycles 2, 14, 15	1041
MDA Multiple Displacement Amplification 2, 3, 14, 15	1042
MLP multilayer perceptron 5, 6, 19	1043
ONT Oxford Nanopore Technologies 3, 4, 9, 10, 16, 17	1044
PacBio Pacific Biosciences 3	1045
PTA Primary Template-directed Amplification 2	1046
SA Supplementary Alignment 16, 17, 20–22	1047
SV Structural Variation 1–5, 9–15, 17, 20, 21	1048
TRA translocation 3, 9, 11	1049
WGA Whole Genome Amplification 1–15, 17–23	1050
	1051
	1052
	1053
	1054
	1055
	1056
	1057
	1058